ChemPubSoc Europe

DOI: 10.1002/chem.201600923

CHEMISTRY A European Journal Communication

Hybrid Micromotors

Autonomously Propelled Motors for Value-Added Product Synthesis and Purification

Sarvesh K. Srivastava* and Oliver G. Schmidt[a]

Abstract: A proof-of-concept design for autonomous, self-propelling motors towards value-added product synthesis and separation is presented. The hybrid motor design consists of two distinct functional blocks. The first, a sodium borohydride ($NaBH_4$) granule, serves both as a reaction prerequisite for the reduction of vanillin and also as a localized solid-state fuel in the reaction mixture. The second capping functional block consisting of a graphene–polymer composite serves as a hydrophobic matrix to attract the reaction product vanillyl alcohol (VA), resulting in facile separation of this edible value-added product. These autonomously propelled motors were fabricated at a length scale down to 400 μm, and once introduced in the reaction environment showed rapid bubble-propulsion followed by high-purity separation of the reaction product (VA) by the virtue of the graphene–polymer cap acting as a mesoporous sponge. The concept has excellent potential towards the synthesis/isolation of industrially important compounds, affinity-based product separation, pollutant remediation (such as heavy metal chelation/adsorption), as well as localized fuel-gradients as an alternative to external fuel dependency.

Since the onset of industrial age, motors have played a key role in the advancement of the human society by converting one form of energy into another. The trend towards greater miniaturization[1] presents a case for autonomously powered micromotors that are capable of converting the energy of chemical fuels or external fields into mechanical motion.[2,3] These microswimmers[4] (with different propulsion mechanisms, such as self-electrophoresis,[5] diffusophoresis,[6] catalytic random fluctuation,[7] or bubble propulsion,[8,9] have been of considerable interest owing to their wide variety of applications in drug delivery,[10] cargo delivery,[11] and next-generation medibots (a multi-specialty microbot for advanced biomedical applications).[12]

The working principle behind bubble-propelled micromotors in particular is to generate a thrust of gases in liquid medium by catalyzing a gas evolution reaction (such as O_2, H_2), thereby propelling the spatially confined asymmetric microstructures in its aqueous reaction environment.[13,14] This has been achieved with the incorporation of certain heterogeneous catalytic layers (Pt, Pd, Ru) in presence of an external fuel (for example, peroxides or hydrazine) to propel these micromotors. A classic example is the oxygen evolution reaction via dissociation of H_2O_2 in the presence of Pt metal catalysts.[15–17] Therefore, there is a constant need to innovate newer reactions and associated materials/design to actively propel these micromotors with an aim to explore novel applications. Recently, Sen et al.[18] reported autonomous motion by a depolymerization-based mechanism of poly(2-ethyl cyanoacrolyte) polymer in aqueous medium. Similarly, studies have been reported for preferential dissolution of magnesium to propel certain microstructures in aqueous environment.[19,20]

The quest for newer reaction mechanisms not only facilitates innovative material/design parameters but is also important in exploring newer applications for such chemically-propelled motor systems. In several of the above mentioned micromotor studies, one may notice that an external fuel gradient is merely required to facilitate the propulsion. Recently, we have reported the wastewater mediated activation of micromotors for pollutant degradation, in which the pollutant mixture itself served as a fuel, thereby limiting external fuel or addition of surfactants.[21] This study happens to be the first scientific report confirming highly efficient pollutant degradation by autonomously propelled micromotors in the volume range of mL along with the absence of surfactants/pH control or addition of external fuel for propulsion. Another interesting study reported by Gao et al[22] demonstrated the Zn-coated micromotor propulsion inside the mouse stomach. Apart from the fact that this may have been the first study reporting an in vivo micromotor application, the very reaction centered around the H_2 evolution by oxidation of Zn metals in presence of HCl warrant its application under acidic conditions (like digestive juices in the stomach with pH 1.5–3.5). Likewise, Soler et al[23] utilized the Fenton reaction for the degradation of Rhodamine 6G in water. The reaction utilizes H_2O_2 in the presence of the Pt-incorporated micromotor structure (along with a Fe layer to execute the Fenton reaction under acidic conditions), thereby providing an autonomous propulsion. These benchmark studies illustrate that the potential application for micromotors can be combined with autonomous propulsion by the virtue of their reaction mechanism. Therefore, it is important to combine the external fuel dependency as an intricate part of the reaction mechanism (if not completely avoidable) to execute/innovate newer applications for such chemical micro

[a] Dr. S. K. Srivastava, Prof. Dr. O. G. Schmidt
Institute for Integrative Nanosciences, IFW Dresden
Helmholtzstrasse 20, 01069 Dresden (Germany)
E-mail: sarvesh.kumar@ifw-dresden.de

Supporting information for this article is available on the WWW under http://dx.doi.org/10.1002/chem.201600923.

swimmers. This trend was well-captured by a recent study done by Yamamoto et al.[24] showing aerobic oxidation of non-toxic alcohols and aldehydes for autonomous propulsion.

In this study, we present the first proof of concept for food-producing micromotors (value-added product synthesis) based on the autonomous propulsion of our hybrid motor setup fabricated both at the macroscopic (1-4 mm) and microscopic (ca. 400 μm) length scale. We synthesized vanillyl alcohol (4-(hydroxymethyl)-2-methoxyphenol) by reduction of vanillin (3-methoxy-4-hydroxy benzaldehyde), which is an important food additive.[25] Vanillin is a phenolic aldehyde extracted from Vanilla beans (*Vanilla planifolia*) as the natural source.[26,27] Several biological and chemical methods have been reported to obtain vanillyl alcohol (VA) from vanillin.[28–30] However, these share an inherent disadvantage of resource intensive extraction, elaborate purification/downstream-processing, or selection/culturing of microbiological strains. Chemical reduction of vanillin with $NaBH_4$ has emerged as a viable alternative (as compared to $LiBH_4$ or $Al(BH_4)_3$) owing to relatively safe handling under industrial conditions.[31] It should be noted that even with $NaBH_4$ mediated reduction, formation of by-products such as borates together with VA requires the use of repeated distillation/downstream processing to obtain a pure product.

Herein, we fabricated autonomously propelled motors capable of converting vanillin into vanillyl alcohol and also promoting their rapid separation (Figure 1). We observed that both the macroscopic (1–4 mm) and microscopic (ca. 400 μm) version of our fabricated micromotor followed similar propulsion characteristics.

We utilized the solvent-dissolved parafilm to create a functional hydrophobic coating (due to the presence of olefin waxes together with graphene) on $NaBH_4$ lumps comprising our motor structure as shown in Figure 1 a. The idea to utilize parafilm was based on the fact that it is readily available along with facile motor fabrication by a polymer dissolution approach.[32] Inclusion of graphene with the parafilm polymer composite was made to utilize the inherent hydrophobic attraction of such mesoporous materials[33] for adsorbing the reaction product, vanillyl alcohol.[34] The resulting reaction involves the reduction of the aldehyde group in vanillin where for every one equivalent of $NaBH_4$, there are four equivalents of hydride.[35] The reduction mechanism involves the transfer of hydride ions from $NaBH_4$ to the carbonyl carbon of the aldehyde group in vanillin, creating a partial positive charge on the carbon of the aldehyde group owing to the greater electronegativity of the oxygen atom, resulting in formation of oxygen–boron bonds (equation of Figure 1 a). Therefore, upon introduction of the motor in the vanillin containing reactant medium, rapid dissociation of $NaBH_4$ results in the reduction of vanillin along with simultaneous propulsion of our bifunctional motors. Once the $NaBH_4$ granule is consumed, in the next phase of the reaction, the oxygen–boron bonds are hydrolyzed in presence of HCl, thereby forming our desired product, vanillyl alcohol (Figure 1 b). Addition of HCl (pH 2.5) not only hydrolyzes the O–B bond in the intermediate but also destroys excess $NaBH_4$ that may be present in the reaction mixture. Finally, as shown in Figure 1 c, owing to the hydrophobic nature of our polymer coating, the resulting product VA was attracted and adhered to it on the top-layer of the reaction mixture promoting easy separation. This can be understood by the fact that the resulting product VA has higher electron density retained by the virtue of the attached aromatic OH groups (lone pairs on the oxygen overlaps with the delocalized ring electron system). Upon completion of the reduction reaction, this enables the product to become attracted towards the graphene–polymer composite (referred hereafter as mesoporous sponge), thereby promoting rapid separation of the high-purity product. This is also important as, in absence of this hydrophobic pull/interaction (keeping other reaction conditions constant), the resulting VA product also contains borates/metaborates as the reaction by-product thereby requiring further downstream processing. The presence of graphene polymer composite in the reaction medium results in faster assimilation of the product (VA) compared to the control sample (Supporting Information, video S4). This can also be understood by the fact that the oxygenated moieties (carbonyl and carboxyl groups) present over the graphene surface acting as a platform for the loading of resulting product via π–π stacking. This warrants the use of graphene polymer composite together with the solid-state fuel for the product synthesis and isolation. Similar motion mechanism was deployed by Ismagilov et al.[36] for artificial millimeter-scale catalytic boat, which can glide across the surface of a liquid via combination of catalytic decomposition of H_2O_2 and relative motion caused by capillary interactions at the fluid–air interface. It is important to note that although kinetic/quantitative analysis may yield greater information about the conversion efficiency and product recovery, it is beyond

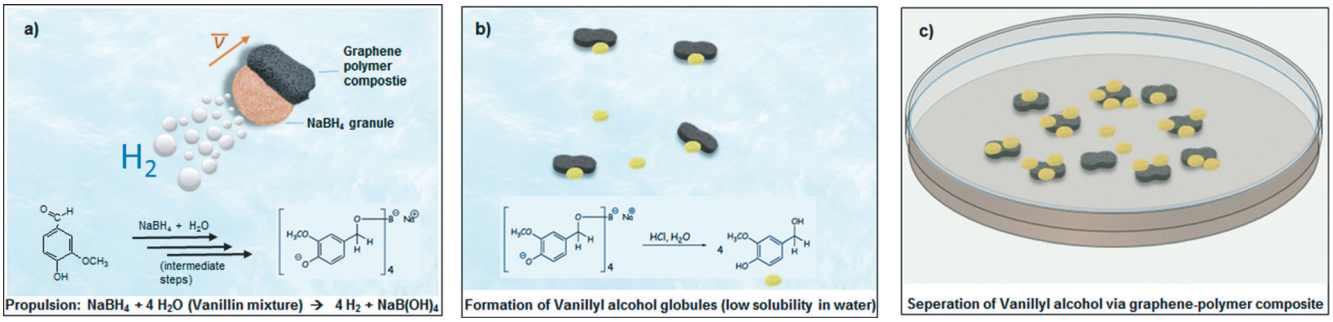

Figure 1. The conversion of vanillin into vanillyl alcohol by autonomously propelled motors.

the rationale of our current proof of concept study. Likewise, in another study by Ikezoe et al.[37] they utilized a peptide–MOF (metal–organic framework) for functional microelectric generators. This was achieved by reorganization of hydrophobic peptides, which could create the large surface tension gradient around the MOF and efficiently powered the translation motion of MOFs. Therefore, we can see that the difference in hydrophobicity/supramolecular interactions towards material synthesis can find a wide range of applications for these micromotors. This is further important to understand that the propulsion of the motors is at the air–liquid interface, that is, essentially 2D. However, to realize the value-added product synthesis and purification, a two-step process takes place: a) product synthesis via complete dissolution of $NaBH_4$ granule in contact with the solution; b) once the $NaBH_4$ granule has reacted completely (dissolved), the graphene–polymer composite interface is in contact with the reaction medium, facilitating product separation.

SEM imaging was carried out to visualize the surface of our polymer matrix (Figure 2). Figure 2a shows the polymer film without any mesoporous graphene, highlighting a comparatively smooth surface. In contrast, Figure 2b shows the surface of the polymer–graphene composite with remarkable changes in terms of surface morphology, with an irregular/rough surface as is the case with mesoporous materials.[38] This graphene–polymer matrix was analyzed post-adsorption of the reaction product VA (Figure 2c). We were able to visualize vanillyl alcohol globules adhered to the surface of the graphene polymer matrix, clearly highlighting their role as mesoporous sponge. Figure 2d shows a representative image for polymer film coated $NaBH_4$ without any inclusion of graphene, corresponding to the SEM surface imaging observed in Figure 2a. From the Supporting Information, video S4, it is important to note that although this satisfies the criteria for being autonomously propelled, in absence of any meaningful functionality, this limits the application of the resulting swimmer system (and micromotors in general). However, incorporation of graphene together with the parafilm polymer matrix (mesoporous sponges) facilitated rapid product separation (via adsorption) once the reaction gets completed (Figure 2e,f). Upon extracting and drying these mesoporous sponges, we can clearly see the pure product vanillin alcohol (as yellow–orange amber-like product) in Figure 2f. The product can then be separated by a simple physical separation method, such as gentle crushing. This is a distinct advantage over conventional synthesis methods where formation of borates as byproduct together with the VA always requires further processing and treatment. Also, in the presence of $NaBH_4$ alone, the resulting product mixture was rather turbid as compared to the visually distinguishable top-layer of the product which gets adsorbed around the mesoporous sponges , thereby requiring subsequent product purification (Supporting Information, Figure S1).

The product adsorption on graphene can be greatly influenced by reaction parameters such as pH and the presence/absence of ionizable species, especially on the adsorption of hydrophobic compounds.[39,40] Furthermore, the ubiquitous natural organic matter (NOM) present in the reaction medium can directly affect product adsorption by decreasing the adsorption sites through competition and pore blockage or increasing adsorption sites owing to its better dispersibility.[41] These properties have in fact made carbon-based adsorbents a lucrative choice for the adsorption and separation of organic compounds such as dyes or pollutants.[42,43] Similarly, we utilized the tendency of polycyclic aromatic units present in the graphene sheets[44] to aggregate our product vanillyl alcohol into columnar stacks, which is due to non-covalent interactions.

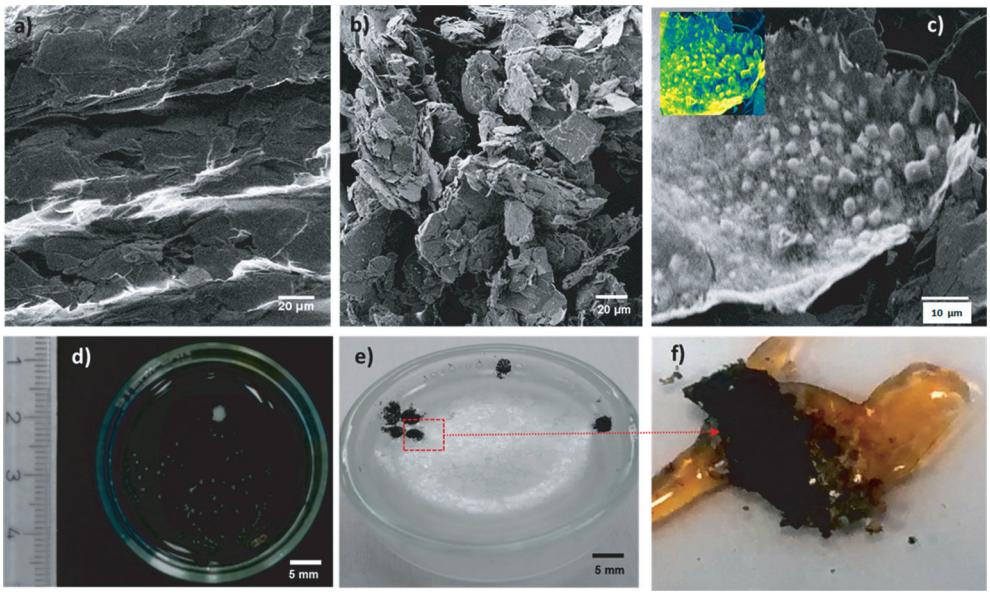

Figure 2. a)–c) SEM surface imaging of a) polymer composite without graphene, b) polymer–graphite composite, and c) polymer–graphite composite after adsorption of the VA product (inset: false color image showing VA globules in green adhered to the graphene polymer surface). d)–f) Representative optical images of d) polymer composite without graphene in its reaction medium, e) polymer–graphite composite with the product VA in the reaction medium, and f) the dried polymer–graphene composite motor covered with pure VA product.

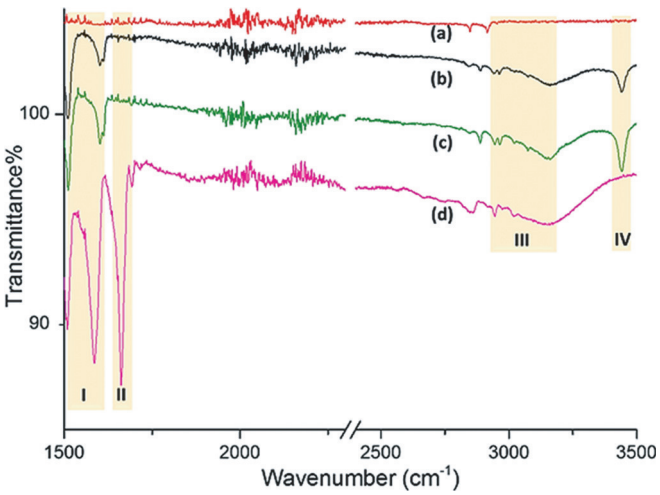

Figure 3. FTIR spectra of a) graphene–polymer control, b) vanillyl alcohol standard, c) graphene–polymer with vanillyl alcohol as adsorbed product, and d) vanillin standard. Regions I–IV highlight different functional groups: I) C=C aromatic ring stretching; II) aldehyde group HC=O; III) phenolic hydroxy and associated alkyl CH_3 group; IV) substituted OH on the benzene ring.

The synthesis and separation of vanillyl alcohol was confirmed by FTIR analysis (Figure 3). Both vanillin and vanillyl alcohol are structurally similar but with a major difference where the C=O stretch of the aldehyde (region II) in vanillin is reduced to OH (region IV) in VA. Figure 3d shows FTIR spectra for vanillin standard, with characteristic absorption of the C=C benzene ring stretching of in the range 1510–1600 cm^{-1} (region I) followed by the HC=O peak of the aldehyde group at about 1660 cm^{-1} (region II).[45] Further, the phenolic ring along with C–H stretching in the methoxy (O–CH_3) associated with the aromatic ring can be attributed to the 2800–3200 cm^{-1} broad stretch (region III), while the ring-associated OH peak is highlighted at about 3400 cm^{-1} (region IV).[46] Compared to this, FTIR spectra for vanillyl alcohol (Figure 3b) showed the C=C peaks for the benzene ring structure (region I) except for the HC=O (aldehyde group, region II). As stated above, this aldehyde group was replaced with the ring-associated OH group, with a characteristic absorption peak observed in region IV of Figure 3b. Finally, we obtained the FTIR spectra of vanillyl alcohol adsorbed graphite sponge (Figure 3c) showing comparable peak positions as compared to vanillyl alcohol (Figure 3b) with distinct absence of the aldehyde group (region II). The peaks were further amplified after the extraction and drying of the top layer of the reaction mixture comprising of VA adsorbed onto the mesoporous sponge showing high purity product separation (Supporting Information, Figure S2). As expected, no major peak was observed for vanillin or VA in case of the graphene–polymer control sample (Figure 3a).

Finally, autonomous motion of food producing motors was studied as shown in Figure 4. The motor design comprised of a bifunctional setup where the lower portion consisting of $NaBH_4$ reacts with the vanillin containing reaction mixture and once it is dissolved, the top hydrophobic graphene–polymer layer comes in contact with the reaction mixture and acts like a mesoporous sponge promoting facile separation of VA. We observed varying velocities in case of graphite deposited and non-deposited motors as shown in Figure 4a,b. When the graphite containing bifunctional $NaBH_4$ lumps were introduced in the vanillin reaction medium, an average velocity of 1.3 mm s^{-1} (Supporting Information, video S1) was observed. We obtained a higher velocity in case of the parafilm polymer coating without graphene ($v = 1.92$ mm s^{-1}), suggesting that certain surface interactions[47,48] can be responsible for slowing down the polymer-graphene motor (Supporting Information, video S2). This is expected, as graphene tends to interact with the vanillyl alcohol reaction product owing to π–π interactions resulting in its separation. Also, given the fact that our autonomous hybrid motor is operational at the air–water interface, surface tension effects will influence the motor movement (along with the hydrogen evolution reaction as the main propelling mechanism), as observed in case of camphor boats[49,50] and solvent-driven gels.[51] The propulsion concept may draw some parallels to a study done by Jin et al.,[52] where they demonstrated a new type of Marangoni propulsion promoting steady velocity for a prolonged period of time owing to the constant supply of fuel vapor through the membrane.

Similar propulsion behavior was observed for the microscaled version (400 μm), as shown in Figure 4c. We observed

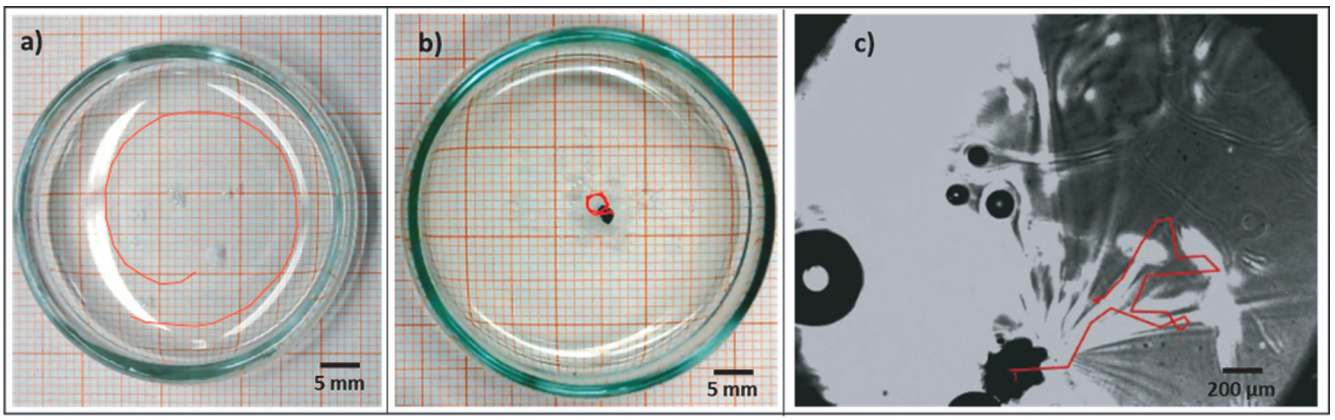

Figure 4. Autonomous propulsion pattern as observed in: a) $NaBH_4$–polymer composite (without graphene), b) $NaBH_4$–graphene–polymer composite, and c) $NaBH_4$–graphene polymer composite at the microscale.

a propulsion speed of 0.4 ± 0.24 mm s^{-1} when the micromotor was introduced into its reactant environment (Supporting Information, video S3). This is comparatively slower than its macroscopic variant probably due to the fact that at macroscopic length scale or large Reynolds numbers, the phoretic effects that power the micromotor motion no longer play an important role. Also, microscale propulsion for a reactant-to-product system may not be as effective as the corresponding larger analogue owing to enhanced viscous, thermal, and interfacial microscale effects.[53,54] Therefore, we observed higher velocity as compared to the phoretic mechanisms in micromotile objects. This also justifies the use of a macroscale architecture for autonomous propulsion based upon its intended application and imparted functionalities. Finally, we believe that such reactant-to-product type micromotors can find interesting applications in production of valuable compounds, removal of pollutants (such as POPs, heavy metals) in water, and may even be extended to biological systems for adsorption of toxins or the sustained release of drugs. Incorporation of high-specificity adsorbents to efficiently trap/purify the compound of interest will greatly influence the development of such autonomous motors from a proof-of-concept study to viable industrial solution in future.

Acknowledgements

S.K.S. would like to thank Deutscher Akademischer Austauschdienst (DAAD)–Leibniz for funding. Also, S.K.S. expresses sincere gratitude to Dr. Mariana Medina-Sánchez and Tony Jaumann for helpful discussions. The authors thank Yan Chen for help with SEM.

Keywords: food production · graphene · hybrid micromotors · polymers · vanillin

[1] P. Peercy, *Nature* **2000**, *406*, 1023 – 1026.
[2] T. E. Mallouk, A. Sen, *Sci. Am.* **2009**, *300*, 72 – 77.
[3] G. A. Ozin, I. Manners, S. Fournier-Bidoz, A. Arsenault, *Adv. Mater.* **2005**, *17*, 3011 – 3018.
[4] S. Sengupta, M. E. Ibele, A. Sen, *Angew. Chem. Int. Ed.* **2012**, *51*, 6378; *Angew. Chem.* **2012**, *124*, 6484.
[5] Y. Wang, R. M. Hernandez, D. J. Bartlett, J. M. Bingham, T. R. Kline, A. Sen, T. E. Mallouk, *Langmuir* **2006**, *22*, 10451 – 10456.
[6] Y. Shi, L. Huang, D. W. Brenner, *J. Chem. Phys.* **2009**, *131*, 014705 .
[7] D. Yamamoto, A. Mukai, N. Okita, K. Yoshikawa, A. Shioi, *J. Chem. Phys.* **2013**, *139*, 034705 .
[8] Y. Mei, A. A. Solovev, S. Sanchez, O. G. Schmidt, *Chem. Soc. Rev.* **2011**, *40*, 2109 – 2119.
[9] M. Manjare, B. Yang, Y. P. Zhao, *Phys. Rev. Lett.* **2012**, *109*, 128305 .
[10] F. Mou, C. Chen, Q. Zhong, Y. Yin, H. Ma, J. Guan, *ACS Appl. Mater. Interfaces* **2014**, *6*, 9897 – 9903.
[11] A. K. Singh, K. K. Dey, A. Chattopadhyay, T. D. Mandal, K. Bandyopadhyay, *Nanoscale* **2014**, *6*, 1398 – 1405.
[12] S. K. Srivastava, M. Medina-Sánchez, B. Koch, O. G. Schmidt, *Adv. Mater.* **2016**, *28*, 832 – 837.
[13] A. A. Solovev, Y. Mei, E. B. Ureña, G. Huang, O. G. Schmidt, *Small* **2009**, *5*, 1688 – 1692.
[14] W. Gao, A. Pei, J. Wang, *ACS Nano* **2012**, *6*, 8432 – 8438.
[15] D. L. Hitt, C. M. Zakrzwski, M. A. Thomas, *Smart Mater. Struct.* **2001**, *10*, 1163 – 1175.
[16] W. F. Paxton, K. C. Kistler, C. C. Olmeda, A. Sen, S. K. St. Angelo, Y. Cao, T. E. Mallouk, P. E. Lammert, V. H. Crespi, *J. Am. Chem. Soc.* **2004**, *126*, 13424 – 13431.
[17] F. Mou, D. Pan, C. Chen, Y. Gao, L. Xu, J. Guan, *Adv. Funct. Mater.* **2015**, *25*, 6173 – 6181.
[18] H. Zhang, W. Duan, L. Liu, A. Sen, *J. Am. Chem. Soc.* **2013**, *135*, 15734 – 15737.
[19] W. Gao, X. Feng, A. Pei, Y. Gu, J. Li, J. Wang, *Nanoscale* **2013**, *5*, 4696 – 4700.
[20] F. Mou, C. Chen, H. Ma, Y. Yin, Q. Wu, J. Guan, *Angew. Chem. Int. Ed.* **2013**, *52*, 7208 – 7212; *Angew. Chem.* **2013**, *125*, 7349 – 7353.
[21] S. K. Srivastava, M. Guix, O. G. Schmidt, *Nano Lett.* **2016**, *16*, 817 – 821.
[22] W. Gao, R. Dong, S. Thamphiwatana, J. Li, W. Gao, L. Zhang, J. Wang, *ACS Nano* **2015**, *9*, 117 – 123.
[23] L. Soler, V. Magdanz, V. M. Fomin, S. Sanchez, O. G. Schmidt, *ACS Nano* **2013**, *7*, 9611 – 9620.
[24] D. Yamamoto, T. Takada, M. Tachibana, Y. Iijima, A. Shioi, K. Yoshikawa, *Nanoscale* **2015**, *7*, 13186 – 13190.
[25] N. J. Walton, M. J. Mayer, A. Vanillin, *Phytochemistry* **2003**, *63*, 505 – 515.
[26] M. D. Sharp, N. A. Kocaoglu-Vurma, V. Langford, L. E. Rodriguez-Saona, W. J. Harper, *J. Food Sci.* **2012**, *77*, C284 – C292 .
[27] A. K. Sinha, U. K. Sharma, N. Sharma, *Int. J. Food Sci. Nutr.* **2008**, *59*, 299 – 326.
[28] A. S. Ranadive, *J. Agric. Food Chem.* **1992**, *40*, 1922 – 1924.
[29] T. Li, J. P. N. Rosazza, *Appl. Environ. Microbiol.* **2000**, *66*, 684 – 687.
[30] J. Overhage, H. Priefert, A. Steinbüchel, *Appl. Environ. Microbiol.* **1999**, *65*, 4837 – 4847.
[31] M. V. Nora De Souza, T. R. A. Vasconcelos, *Appl. Organomet. Chem.* **2006**, *20*, 798 – 810.
[32] B. A. Miller-Chou, J. L. Koenig, *Progress in Polymer Science (Oxford)* **2003**, *28*, 1223 – 1270.
[33] H. Bi, X. Xie, K. Yin, Y. Zhou, S. Wan, L. He, F. Xu, F. Banhart, L. Sun, R. S. Ruoff, *Adv. Funct. Mater.* **2012**, *22*, 4421 – 4425.
[34] O. Leenaerts, B. Partoens, F. M. Peeters, *Phys. Rev. B* **2009**, *79*, 235440 .
[35] M. R. Johnson, B. Rickborn, *J. Org. Chem.* **1970**, *35*, 1041 – 1045.
[36] R. F. Ismagilov, A. Schwartz, N. Bowden, G. M. Whitesides, *Angew. Chem. Int. Ed.* **2002**, *41*, 652 – 654; *Angew. Chem.* **2002**, *114*, 674 – 676.
[37] Y. Ikezoe, J. Fang, T. L. Wasik, T. Uemura, Y. Zheng, S. Kitagawa, H. Matsui, *Adv. Mater.* **2015**, *27*, 288 – 291.
[38] P. Innocenzi, L. Malfatti, D. Carboni, *Nanoscale* **2015**, *7*, 12759 – 12772.
[39] F. Liu, J. Zhao, S. Wang, P. Du, B. Xing, *Environ. Sci. Technol.* **2014**, *48*, 13197 – 13206.
[40] X. Wang, J. Lu, B. Xing, *Environ. Sci. Technol.* **2008**, *42*, 3207 – 3212.
[41] L. L. Ji, W. Chen, Z. Y. Xu, S. R. Zheng, D. Q. Zhu, *J. Environ. Qual.* **2013**, *42*, 191 – 198.
[42] P. M. Budd, B. S. Ghanem, S. Makhseed, N. B. McKeown, K. J. Msayib, C. E. Tattershall, *Chem. Commun.* **2004**, 230 – 231.
[43] P. M. Budd, E. S. Elabas, B. S. Ghanem, S. Makhseed, N. B. McKeown, K. J. Msayib, C. E. Tattershall, D. Wang, *Adv. Mater.* **2004**, *16*, 456 – 459.
[44] N. B. McKeown, P. M. Budd, *Chem. Soc. Rev.* **2006**, *35*, 675 – 683.
[45] H. Peng, H. Xiong, J. Li, M. Xie, Y. Liu, C. Bai, L. Chen, *Food Chem.* **2010**, *121*, 23 – 28.
[46] F. Kayaci, T. Uyar, *J. Agric. Food Chem.* **2011**, *59*, 11772 – 11778.
[47] E. Lauga, A. M. J. Davis, *J. Fluid Mech.* **2012**, *705*, 120 – 133.
[48] K. Ichimura, *Science* **2000**, *288*, 1624 – 1626.
[49] S. Nakata, Y. Iguchi, S. Ose, M. Kuboyama, T. Ishii, K. Yoshikawa, *Langmuir* **1997**, *13*, 4454 – 4458.
[50] H. Kitahata, S. Hiromatsu, Y. Doi, S. Nakata, R. M. Islam, *Phys. Chem. Chem. Phys.* **2004**, *6*, 2409 – 241.
[51] R. Sharma, S. T. Chang, O. D. Velev, *Langmuir* **2012**, *28*, 10128 – 10135.
[52] H. Jin, A. Marmur, O. Ikkala, R. H. A. Ras, *Chem. Sci.* **2012**, *3*, 25 – 26.
[53] Y. Hong, D. Velegol, N. Chaturvedi, A. Sen, *Phys. Chem. Chem. Phys.* **2010**, *12*, 1423 – 1435.
[54] Y. G. Tao, R. Kapral, *J. Chem. Phys.* **2009**, *131*, 024113 .

Received: February 26, 2016
Revised: April 3, 2016
Published online on May 24, 2016